

ACCEPTED MANUSCRIPT

A first-principles study of magnetic properties of $\text{Zn}_{0.94}\text{Mg}_{0.01}\text{Mn}_{0.05}\text{O}$

To cite this article before publication: Izzet Parug Duru *et al* 2019 *Mater. Res. Express* in press <https://doi.org/10.1088/2053-1591/ab63f6>

Manuscript version: Accepted Manuscript

Accepted Manuscript is “the version of the article accepted for publication including all changes made as a result of the peer review process, and which may also include the addition to the article by IOP Publishing of a header, an article ID, a cover sheet and/or an ‘Accepted Manuscript’ watermark, but excluding any other editing, typesetting or other changes made by IOP Publishing and/or its licensors”

This Accepted Manuscript is © 2019 IOP Publishing Ltd.

During the embargo period (the 12 month period from the publication of the Version of Record of this article), the Accepted Manuscript is fully protected by copyright and cannot be reused or reposted elsewhere.

As the Version of Record of this article is going to be / has been published on a subscription basis, this Accepted Manuscript is available for reuse under a CC BY-NC-ND 3.0 licence after the 12 month embargo period.

After the embargo period, everyone is permitted to use copy and redistribute this article for non-commercial purposes only, provided that they adhere to all the terms of the licence <https://creativecommons.org/licenses/by-nc-nd/3.0>

Although reasonable endeavours have been taken to obtain all necessary permissions from third parties to include their copyrighted content within this article, their full citation and copyright line may not be present in this Accepted Manuscript version. Before using any content from this article, please refer to the Version of Record on IOPscience once published for full citation and copyright details, as permissions will likely be required. All third party content is fully copyright protected, unless specifically stated otherwise in the figure caption in the Version of Record.

View the [article online](#) for updates and enhancements.

A first-principles study of magnetic properties of $\text{Zn}_{0.94}\text{Mg}_{0.01}\text{Mn}_{0.05}\text{O}$

I.P. Duru¹, E. Ozugurlu², L. Arda^{3*}

¹Marmara University, Department of Physics, Faculty of Science and Literature, 34722, Kadikoy, Istanbul, Turkey

²Istanbul Technical University, Department of Mathematics, 34469, Istanbul, Turkey

³Bahcesehir University, Faculty of Engineering and Natural Sciences, Department of Mechatronic Engineering, 34349, Besiktas, Istanbul, Turkey

ABSTRACT

The structural and magnetic properties of Mg/Mn-doped ZnO were investigated by the first-principles study and Monte Carlo methods (MCs). Applying magnetic force theorem (MFT) and using Kohn-Sham orbitals in the GGA-PBE scheme, the exchange coupling parameters (J) were calculated to figure out the magnetic interactions between atomic sites. Mn-Mg volume clustered (C1) ferromagnetic (FM) state was preferred; herewith, the calculated magnetic moment of Mn was $4.19\mu_B$ and Mg has the highest moment value when clustered with Mn ions. Nearest Mn ions interacted antiferromagnetic (AFM) despite the increasing distance lead them to be in FM. However, AFM/FM was originated from the p-d hybridization, superexchange interaction and direct exchange between distant Mn ions. In addition, the Curie temperature (T_c) was calculated as 311K using averaged magnetization and magnetic susceptibility via MC.

Keywords: Mg/Mn-doped ZnO, first-principles study, density functional theory, GGA+PBE, Monte Carlo methods, room temperature ferromagnetism

*Corresponding author at Ciragan Cad. Osmanpasa Mektebi Sok., 34349 Besiktas Istanbul, Turkey. Tel.: +90 212 3810558; fax: +90 212 3810000.
E-mail address: lutfi.arda@eng.bau.edu.tr (L. Arda).

1. Introduction

Zinc oxide (ZnO) has become an important semiconductor material with a wide direct band gap of 3.37 eV and a large exciton binding energy of 60 meV at room temperature [1-17]. ZnO crystal with wurtzite geometry is an II-VI compound semiconductor [18, 19]. These features make it broadly useful in optoelectronic devices and photoelectric applications, namely, gas sensors, transparent conductive oxides, and light-emitting devices [19 - 22]. In this perspective, metal oxides are particularly favorable materials used in primary technologies such as photovoltaics or solar fuel production as well as in energy storage technologies (e.g. batteries) [6, 13]. Besides, ZnO can be turned into a diluted magnetic semiconductor (DMS) via doping certain concentrations of impurity atoms, especially transition metals, and gain significant magnetic properties. Ferromagnetism (FM) at room temperature (RT) provides a wide area for device applications [11-12, 14-15, 23, 24, and 25]. Since FM behavior almost induced by structural and electronic properties of a material (also ZnO), previous and latest theoretical studies focused on these features to investigate the origin of magnetism and interested properties. Xue et al. found that Ni-3d and O-2p states had a strong hybridization near Fermi level in Ni-doped zinc blende (ZB) ZnO and magnetic moments mainly originated from the unpaired Ni 3d orbitals, and the O 2p orbitals contribute a little to the magnetic moments [26]. Khalid et al. [11] observed shifting of Fermi level in the conduction band with increasing metal concentrations and metal-doped ZnO having ferromagnetic nature via DFT with generalized gradient approximation (GGA). Moreover, Fedorov et al. [12] reported ferromagnetism induced by intrinsic defects in ZnO (DFT-GGA). Mamamouni et al. [14] focused on the electronic structure of the V-doped ZnO system using DFT resulting in Ruderman-Kittel-Kasuya-Yosida (RKKY) interaction and the atomic spin polarization of V were the key factors for the presence of ferromagnetism in V-doped ZnO system. However, at

1
2
3 room temperature, particle size sensitive ferromagnetism was observed for ZnO
4 nanoparticles and oxygen vacancies played a crucial role in the size of the nanoparticles
5 [15]. Cao et al. [23] interested in the electronic and magnetic properties of (Mn,Fe)-co-doped
6 ZnO within the GGA and GGA+U schemes resulting in a ground state ferromagnetic ordering,
7 which was mediated by double exchange mechanism. Electronic and magnetic properties of
8 the Mn-doped ZnO semiconductor were calculated by the full-potential linearized augmented
9 plane wave (FP-LAPW) method with the local spin density approximation (LSDA) and the
10 modified Becke–Johnson (mBJ) potential considering magnetic interaction between the Mn
11 atoms, both the near and far positions exist [24]. Recently, El Haimour et al. [25] investigated
12 the optical, electronic, and magnetic properties (Curie temperature, magnetic moment) of $Zn_{1-x}M_xO$
13 ($M = Fe\ 5\%$, $Co\ 1\%$, $Cr\ 5\%$, and $Mn\ 5\%$) by KKR method and deduced that TM
14 impurities induce ferromagnetism with the Curie temperature closer to room temperature. In
15 contrast, Liu et al. [27] reported that Mn-doped ZnO exhibited antiferromagnetism, only Co-
16 Mn-co-doped ZnO possessed high T_c of better ferromagnetism rather than Co or Mn-doped
17 ZnO. Gallegos et al. [28] showed that magnetic moment lowered by the presence of oxygen
18 vacancies, which could lead to a phase transition from FM to AFM. According to Goumrhar
19 et al. [29], 6% Mn doping caused ferromagnetic behavior, which was originated from double
20 exchange interaction, p-d hybridization. On the other hand, Mg doping to ZnO increased
21 bandgap [30-32]. Singh and Chae [33] showed that nanoparticles of MgO exhibited
22 ferromagnetism and improved optical and dielectric behavior. Chen et al. [34] showed that
23 under external electric field, was used to tune magnitude of band gap and band dispersion,
24 ZnMgO monolayer is a direct band gap semiconductor [30]. Özgür et al. [4] calculated the band
25 gap of ZnMgO as 3.37 eV and showed that their results were consistent with the experimental
26 results.
27
28
29
30
31
32
33
34
35
36
37
38
39
40
41
42
43
44
45
46
47
48
49
50
51
52
53
54
55
56
57
58
59
60

1
2
3 Present work presents a relatively wide content focused on the magnetic properties
4 through structural analysis of $\text{Zn}_{0.94}\text{Mg}_{0.01}\text{Mn}_{0.05}\text{O}$ based on the experimental data. Structural
5 information and magnetic moments of four distinct distributions of dopants (Mg/Mn) as
6 surface cluster (L1)/surface non-cluster (L2), volume cluster (C1), and volume non-cluster
7 (C2) were obtained by performing density functional theory calculations (DFT) with the
8 generalized gradient approximation (GGA) in the Perdew-Burke-Ernzerhof (PBE) scheme.
9 The magnetic force theorem (MFT) was used to calculate exchange couplings J , between
10 atoms in lattice sites. Thus, the most favored magnetic state was determined and the origin of
11 magnetism was revealed. Finally, a fastened procedure was applied to calculate the Curie
12 temperature (T_c) by Monte Carlo methods based on the Metropolis algorithm since RT
13 ferromagnetism was demanded materials.
14
15
16
17
18
19
20
21
22
23
24
25
26
27
28
29

30 **1.1. Computational Details**

31
32 The effects of dopant concentration and site positioning of impurity ions to magnetic
33 behavior were determined by performing first-principles calculations using the OpenMx 3.8
34 package [35]. Two main modes, namely, volume and surface cases, were devised to modestly
35 specify the most preferable formation of doped structure. Such an exertion would provide
36 essential information about the distribution tendency of the impurity atoms either layered or
37 cubed. Besides, the nearest neighboring of Mn ions as clusters point out the Mn-O-Mn
38 bonding while only Zn-O-Mn bonding should be apparent for the parted Mn ions. Previous
39 studies showed that clustering of doped atom is preferable in contrast to unclustered/randomly
40 distributions (for ZnNiO [36-41]; for ZnMnO [24, 27-29, 42-47]; for ZnMgO [4, 30-34, 40,
41 48]; for ZnCrO [25, 49]; for ZnCoO [27, 29, 37, 47, 50]) even though it is not sufficiently
42 evident for Mg/Mn doped ZnO such a low concentration of dopants. Hence, Mg was
43 incorporated into the ZnMnO for both cases such as closest and distant to Mn ions clusters.
44
45
46
47
48
49
50
51
52
53
54
55
56
57
58
59
60

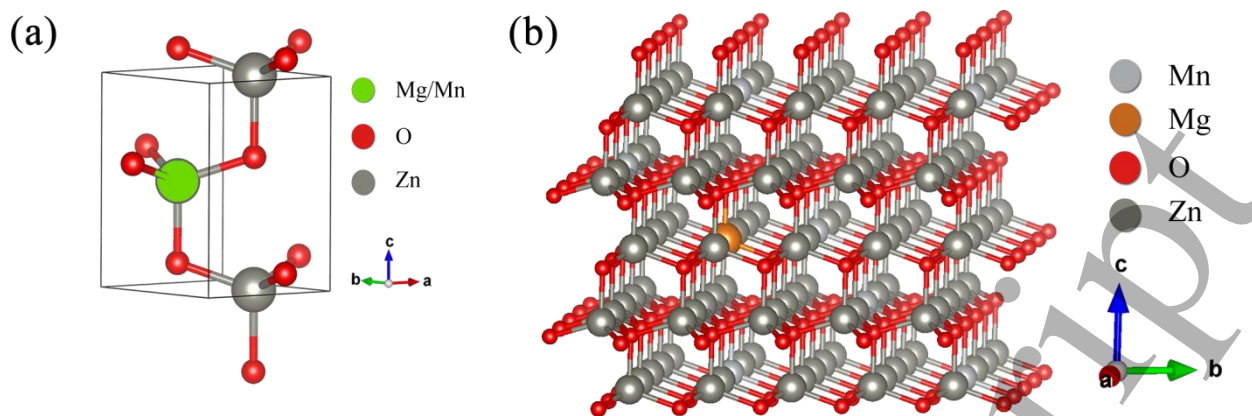


Figure 1. (a) Unit cell (b) Supercell of hexagonal ZnO

Geometry optimized atomic positions were initially assigned for both antiferromagnetic (AFM) and ferromagnetic (FM) states of spin-polarized energy calculation via solving Kohn-Sham equations using plane-wave pseudopotentials and pseudoatomic orbitals briefly PAOs basis functions of Zn, Mn, Mg and O [51-54]. GGA was used in the Perdew-Burke-Ernzerhof (PBE) [55] scheme for exchange-correlation function assigning SCF criteria as $1.0E-7$ Ha and k-points has been set to $12 \times 12 \times 4$ for Monkhorst-Pack grid [56] restricting the energy range of density of states between -20 and 20 eV. However, AFM and FM phases were investigated dealing with collinear spins along c direction neglecting spin-orbit interaction due to its trivial contribution to the current structure. We determined exchange coupling constants, J_{ij} , between strongly localized moments of different atomic sites by a magnetic force theorem [57] since total energy could not be known in advance. For a better magnetic characterization of many-particle systems, Heisenberg model can be used with predetermined exchange coupling constants which can be obtained via DFT calculations. Lack of direct experimental measurement, in particular, to determine these parameters, several approaches took place [58-62] and one of them was based on LDA through magnetic phase states (MTS) which were detailed by Zeng et al. [58] in a theoretical manner. Boukhvalov et al. [59] reported a Hubbard correction (U) included the LDA method, namely, LDA+U to handle Heisenberg exchange coupling parameters (J) more realistic. They

calculated effective J parameters for Mn clusters. A Green's function formalism was developed in order to be applicable to a non-orthogonal basis set, on account of a better estimation of exchange couplings. Equation (1), which was arisen from rigid spin approximation (RSA) applied to DFT ground state [42-45], was used to calculate J_{ij} between i and j sites where G_{ij} denotes the Kohn-Sham orbital states related spin-dependent single-particle Green's function, and V_{ij} is the exchange interaction potential [63].

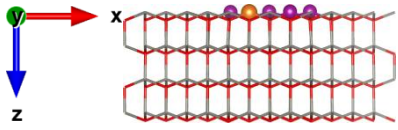
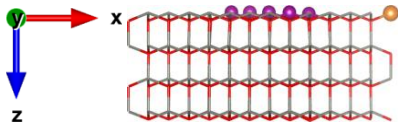
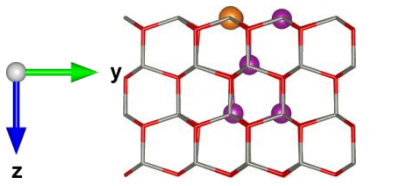
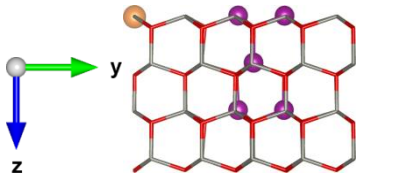
$$J_{ij} = \frac{1}{2\pi} \int^{\varepsilon_F} d\varepsilon \text{Tr} [\hat{G}_{ij}^{\uparrow} \hat{V}_j \hat{G}_{ji}^{\downarrow} \hat{V}_i] \quad (1)$$

2. Results and Discussions

ZnMgMnO supercell (P6₃mc space group) was constructed based on experimental lattice parameters (given in Table 1) via packaging 5×5×2 of the ZnO unit cell having totally 200 atoms. Mn and Mg concentrations were fixed to 5% and 1%, respectively during simulations. Composition with optimized Mn/Mg positions in hexagonal structure to total energies was also given in Table 1. L1, L2, C1, and C2 are labels set to represent cluster/non-cluster surface layers and cubed volume distributions. Only Mn cluster with Mg cluster/non-cluster distribution was adequately built to investigate the electronic and magnetic properties due to a common assent, which suggested that the behavior of dopant ions was clustering in a host material. The energy difference $\Delta E = E_{AFM} - E_{FM}$ of these structures indicates that the favorable magnetic phases are either ferromagnetic (FM) or antiferromagnetic (AFM). $(\Delta E)_{L1} = 1.947$ meV and $(\Delta E)_{L2} = 4.60$ meV refer to an FM ground state for both surface layered distributions; herewith, non-clustered Mg possessed a bigger energy difference. In C1 and C2 cases, $(\Delta E)_{C1}$ and $(\Delta E)_{C2}$ were found to be 11.6 meV and 6.5 meV, respectively. Note that ΔE of volume distributions was higher than surface ones; in fact, volume clustering had the highest value comparing with the rest of the studied distributions. In addition, since physical

properties are mostly related to structural content, bond angles and bond lengths were calculated by a self-coded script importing geometry optimized L1, L2, C1, and C2 crystallographic data (see Table 2 and Table 3).

Table 1. Dopant distribution and lattice parameters with corresponding energies of 5% Mn and 1% Mg-doped ZnO. Cluster and non-cluster emphasize the absolute location of the Mg atom. Mn and Mg atoms were represented by purple and orange spheres respectively; meanwhile, it was preferred to illustrate Zn and O by gray and red sticks.

Superlattice	Dopant Dist.	Label	$\Delta E/p.a.$ (meV)	Type
	Cluster (Layer)	L1	1.947	FM
	Non-Cluster (Layer)	L2	4.60	FM
	Cluster (Cubed)	C1	11.6	FM
	Non-Cluster (Cubed)	C2	6.5	FM

*Experimental lattice parameters ($a=3.237$ (Å), $c=5.195$ (Å)) were obtained from [64]

According to Table 2, the closest connection was observed between Mn and O ions through geometry optimized supercell. In addition, other Mg-O and Zn-O couples inherently came close to each other rather than other couples such as Mn-Mn, Zn-Mn. For instance, Mn-Mn possessed far more distance directly related to Mn-O couples getting close. Besides, experimental bond length [65] had the best fit for Mg-O bond length in L2 (1.952317 Å) distribution in which Mg occupied the most distant location to the Mn cluster.

Table 2. Bond lengths (Å) of surface/volume cluster/non-cluster 5% Mn and 1% Mg doped ZnO. Cluster and non-cluster emphasize the absolute location of the Mg atom.

A-B	L1	L2	C1	C2
Mn-O	1.830803	1.832177	1.806310	1.818967
Mn-Mn	2.912766	2.881406	2.956275	2.948955
Mn-Zn	3.173357	3.081449	3.129474	3.130044
Zn-O	1.933964	1.928778	1.929200	1.935550
Mg-Mn	3.200071	8.724499	3.174350	11.411750
Mg-O	1.940216	1.952317	1.930428	1.947546
Mg-Zn	3.193412	3.168307	3.172892	3.161646
Zn-Zn	3.157933	3.161942	3.157375	3.152024
O-O	3.034565	3.056118	2.997663	2.997219

*Experimental bond length of Zn/Mg/Mn-O 1.9751Å.

Bond angles and standard deviation of optimized geometries were calculated by averaging angles for each species existing in ZnMgMnO the structure including standard deviation per means of bond angles. The interdependency of these angles and lengths determines the variety of the exchange interactions, both directly and indirectly, due to the electronic occupancy of atomic orbitals. Thus, the hybridizing of certain ones (p-d) should control the atomic magnetic behavior of the system that is induced by the structural properties of materials like bond angles. According to Table 3, label (2) and label (8) bond angles did not exist in the L2 and C2 distributions due to the distant position. Even though, one does not have a piece of exact information, in which atoms make certain bonds to dramatically contribute to the magnetic phase of the system. Indirect exchange mechanisms, in particular, superexchange and double exchange determining magnetic behavior, ferromagnetic or antiferromagnetic, naturally occurred through A-O-B like triple bounded via oxygen (A and B should be the different ion of the same atom or totally different atoms) [66-68].

Table 3. Averaged bond angles ($\bar{\theta}$), standard deviations ($\delta\theta$) and standard deviation per mean of bond angle $\delta\theta/\bar{\theta}$ of surface/volume cluster/non-cluster 5% Mn and 1% Mg doped ZnO. Cluster and non-cluster emphasize the absolute location of the Mg atom.

A-B-C	L1(°)	L2(°)	C1(°)	C2(°)
O-Zn-O (1)	109.3403	109.3593	109.3679	109.3623
O-Mg-O (2)	111.7121	-	111.2767	-
O-Mn-O (3)	110.4099	110.9802	110.0351	109.3771

Zn-O-Zn (4)	109.4175	109.3459	109.3604	109.3669
Zn-O-Mn (5)	111.9530	112.1984	112.217	112.1668
Zn-O-Mg (6)	108.5981	109.5376	110.1002	109.4825
Mn-O-Mn (7)	109.7866	109.9598	109.3726	110.0091
Mn-O-Mg (8)	112.4028	-	110.9134	-

Standard deviation ($\delta\theta$) –Standard deviation per average bond angle $\delta\theta/\bar{\theta}$

1	$\delta\theta$	1.7083	1.7410	1.88305	1.9309
	$\delta\theta/\bar{\theta}$	0.0156	0.0159	0.0172	0.0177
2	$\delta\theta$	1.0439	-	0.89422	-
	$\delta\theta/\bar{\theta}$	0.0093	-	0.008	-
3	$\delta\theta$	3.3258	3.7128	4.11764	3.6634
	$\delta\theta/\bar{\theta}$	0.0301	0.0335	0.0374	0.0335
4	$\delta\theta$	1.9521	1.9577	1.95381	1.9655
	$\delta\theta/\bar{\theta}$	0.0178	0.0179	0.0179	0.0180
5	$\delta\theta$	2.9075	3.2011	3.0474	2.8824
	$\delta\theta/\bar{\theta}$	0.026	0.0285	0.0272	0.0257
6	$\delta\theta$	3.1714	2.1002	1.40245	1.906
	$\delta\theta/\bar{\theta}$	0.0292	0.0192	0.0127	0.0174
7	$\delta\theta$	3.1539	3.9608	3.48413	2.0490
	$\delta\theta/\bar{\theta}$	0.0287	0.0360	0.0319	0.0186
8	$\delta\theta$	2.573	-	2.3956	-
	$\delta\theta/\bar{\theta}$	0.0229	-	0.0216	-

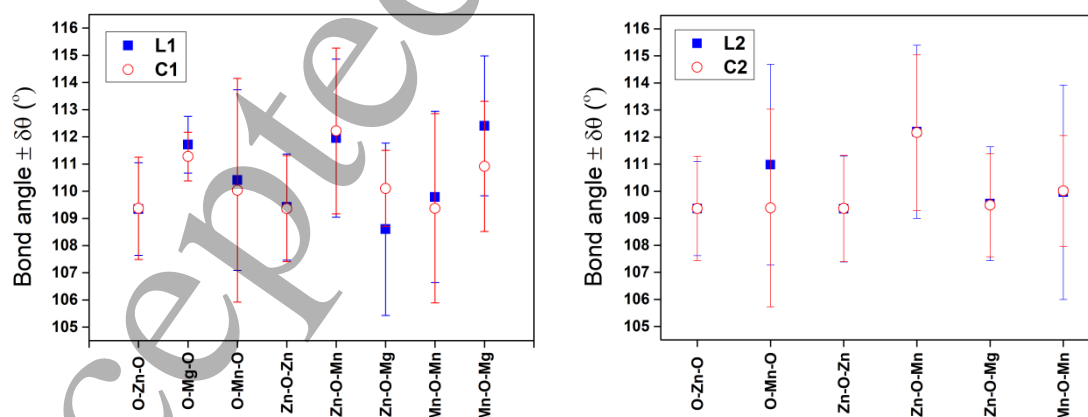


Figure 2. Average bond angles with a standard deviation of L1/C1 and L2/C2 distributions

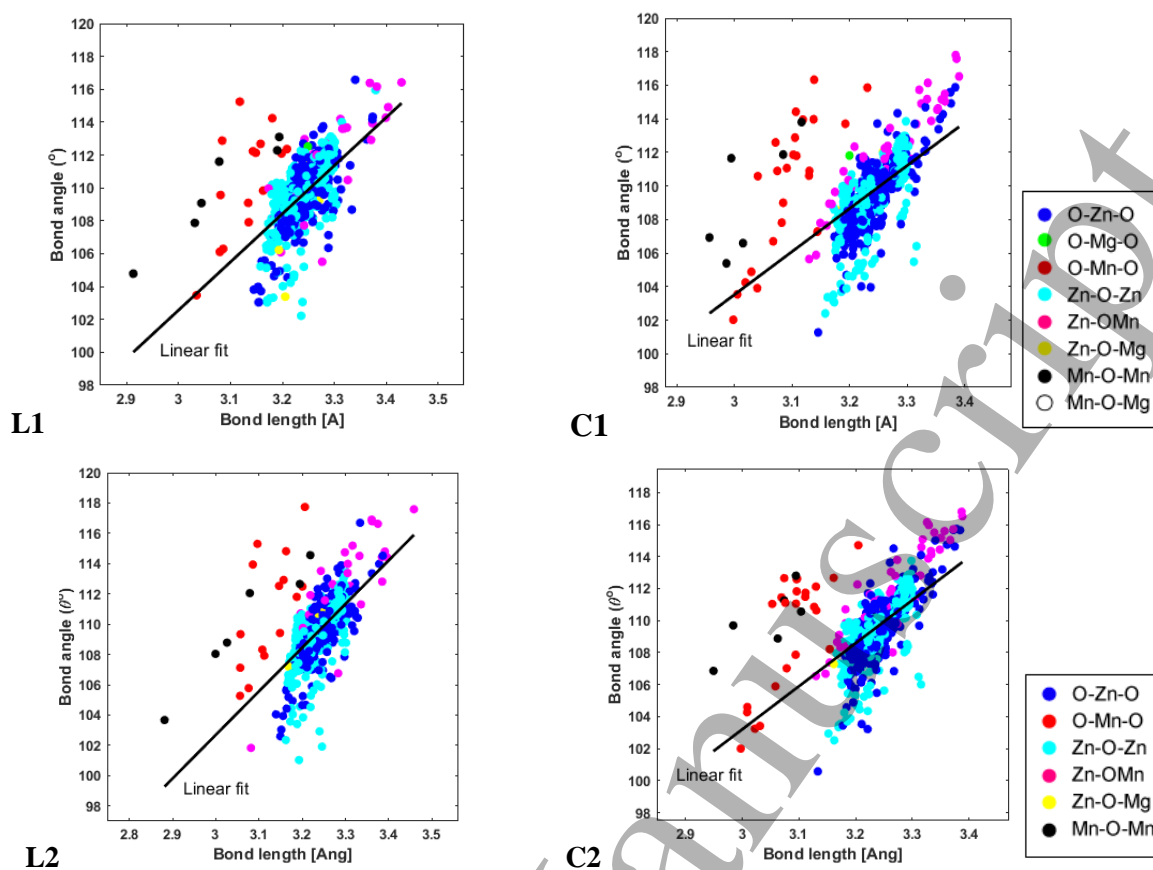


Figure 3. Bond angles – bond length (fingerprint) of surface/volume cluster/non-cluster 5% Mn and 1% Mg doped ZnO. Cluster and non-cluster emphasize the absolute location of the Mg atom.

Averaged bond angles were shown in Fig. 2 with standard deviation. In non-clustered distributions, whole angle values of L2 and C2 practically overlap except O-Mn-O; on the contrary, bond angles of L1 and C1 are mostly different from each other except O-Zn-O and Zn-O-Zn. These triples possessed very close values for all distributions, most probably, according to the low dopant concentration and clustered Mn ions. Figure 3 illustrates the A-C bond length corresponding to the A-B-C bond angle with a linear fit. Note that variation in bond angle may not affect the bond length of any third-part atom which is bounded to B. As shown in Fig. 3, one can deduce that existence of Mn ions distinguishably reduces not only reduce bond angles and bond lengths but also lead to Mn-Mn direct coupling (see Mn-O-Mn and O-Mn-O data). However, other couplings and bonds including also Mg can be seen as a part of a fingerprint-like distribution that forms the 'spinal' of the system; besides, L1, C1 and L2, C2 resemble each other.

Orbital and total magnetic moments were obtained in terms of μB from spin-polarized DFT calculations point out the effect of clustering and non-clustering configurations even

surface and volume type. In case of C1, the magnetic moment of Mn, Mg, Zn, and O were found to be $4.197248666\mu_B$, $0.020923716\mu_B$, $0.003242702\mu_B$, and $0.017441612\mu_B$, where Mn is the main contributor mostly from all five d-orbitals that almost possessed equal values. Similar results were obtained from other configurations. Mg of C1 or L1 configurations had larger magnetic moments than C2 or L2 configurations. Moreover, not only Mn moment values were lowest for clustered structures but also Mn in C1 possessed the lowest value. In addition, magnetic moments are in agreement with the experimental findings of nanoparticles [23, 25, 27, and 69]. As a secondary dopant and an eligible band-gap tuner, Mg ion also affected the strength of the magnetic state when its location changed; on the other hand, magnetic moment differed according to the distance of Mg-Mn pairs (Fig. 4).

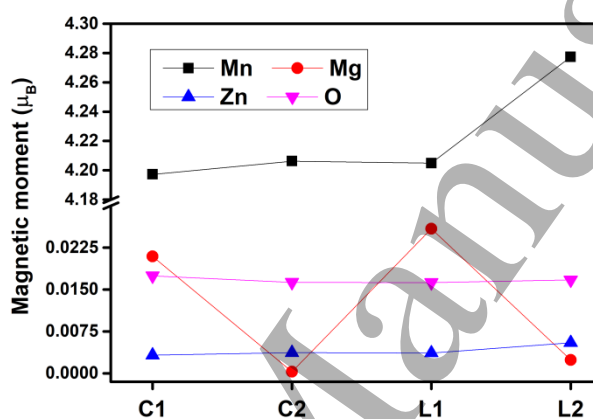


Figure 4. Magnetic moments of host and guest atoms for C1, C2, L1 and L2 states of 5% Mn and 1%Mg doped ZnO

Further magnetic properties were investigated via calculating J exchange coupling constants between host and guest atoms to reveal direct and indirect exchange interactions, especially superexchange, double-exchange, and orbital hybridizations which lead the material gain ferromagnetic (including ferrimagnetism) behavior because of impurity atoms. Since C1 possessed the most stable ferromagnetism, we calculated J values only for this state. Bond lengths, the sign of exchange interaction (AFM/FM), and J values are given in Table 4. Besides, detailed information on distance and neighboring oxygen type reveals the correlation between structural property and magnetic behavior; in fact, orbital hybridizations and indirect mechanisms should be appropriately explained. One can remember that there are 5 Mn atoms in which 4 of them were located around an Mn atom in cubed volume configuration. 2.99412 \AA and 2.98579 \AA distant Mn-Mn pairs showed strong AFM as -21.76 meV and -25.93 meV , respectively while 5.09671 \AA and 5.07144 \AA distant pairs interacted antiferromagnetically with energies of -3.82155 meV and -4.12166 meV . In contrast to the former, furthest distance of Mn-Mn pairs as 5.88841 \AA contributed to FM behavior even if it is weak; herewith Mg-Mn

pairs possess approximately the same sign and strength. However, Mn-O (count 4 times for an Mn) pairs showed FM behavior almost approximately 10 times of furthest distance of Mn-Mn pairs. Exchange energy of Mn-O pairs very weakened after 3 Å so they could not significantly contribute to the overall FM as can be seen in Fig. 5b. Distant dependent variations of exchange coupling J corresponding to Mn-Mn and Mn-O pairs were shown in Figs. 5a-b, respectively.

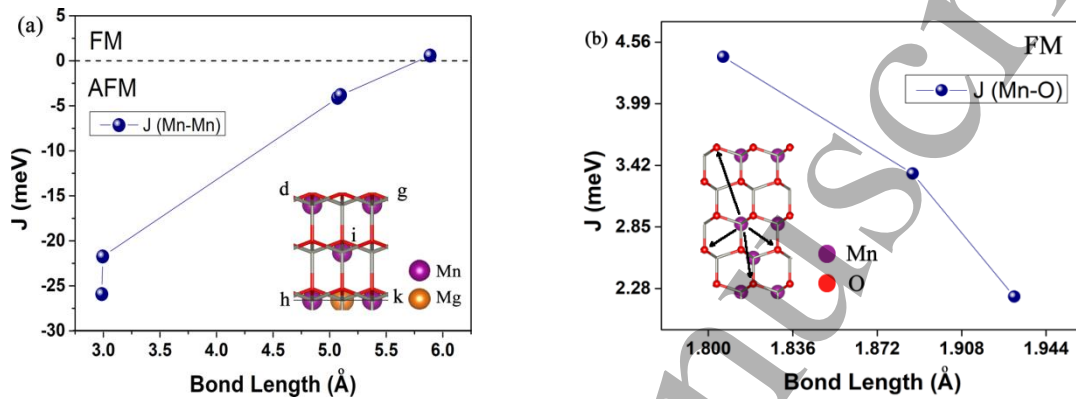


Figure 5. J values versus bond lengths of (a) Mn-Mn pairs (b) Mn-O pairs

Table 4. Bond length (Å), exchange couplings J (meV) and interaction type of C1 state of 5% Mn and 1% Mg doped ZnO.

A-B	Bond length (Å)	Bond angle ($^{\circ}$)	J (meV)	Exchange interaction
Mg-O ^a	2.03695	-	-0.64512	AFM
Mg-O ^{b,c}	1.93301 ^b , 1.93029 ^c	-	-0.6E-3 ^{b,c}	AFM
Mn ^d -O ^a	1.80631	-	4.4241	FM
Mn ^d -O ^{e,f}	1.93042 ^e , 1.88709 ^f	-	2.2062 ^e , 3.3441 ^f	FM
Mn ^d -Mn ^g	2.99412	111.6516	-21.7587	AFM
Mn ^d -Mn ^h	5.09671	175.6310	-3.82155	AFM
Mn ^d -Mn ⁱ	2.98579	105.3924	-25.9286	AFM
Mn ^g -Mn ^k	5.07144	176.7154	-4.12166	AFM
Mn ^g -Mn ^h	5.88841	-	0.566168	FM
Mg-Mn ^d	3.17440	111.2324	0.579357	FM
Mg-Mn ^j	3.23021	108.3730	0.330742	FM
Mg-Zn	3.17289	170.9862	-2.5E-5	AFM
Mn-Zn	3.38378	117.7894	0.06064	FM
Zn-Zn	5.21290, 3.157375	175.9059	-3.78329E-05, ~0	AFM

^aMn neighboring oxygen, ^{b,c}Zn neighboring oxygen, ^dMn neighboring oxygen, ^{e,f}Zn neighboring oxygen

The bond length of Mg-Mn neighboring oxygen couple is evidently longer than Mg-Zn neighboring oxygen couple and AFM interaction exists between Mg-O even Mn mediated a more energetic exchange value relative to Zn. However, Mn-O has an FM type interaction whose strength decreases in direct proportion with increasing distance between these atoms. FM interaction shows dominancy against AFM(10 times larger) when only MgO and MnO couples are compared. On the other hand, when the bond angle of Mn-O-Mn was increased, AFM interaction weakened up to nearly 7 times except for distant Mn ions in which FM interaction exists. However, magnetic strengths of Mg-Mn couples were found to be high as distant Mn-Mn pairs. Mg which was bonded to Zn oxygen (Mg-O^{b,c}) and Mg-Zn, slightly contributed to the exchange mechanism of the whole system as AFM and FM state, respectively.

The intriguing nature of DMS materials, which are constructed by doping 3d or 4f TM elements forming impurities or pioneering vacancies, provided many question marks about the origin of magnetism. Several models such as p-d hybridization, superexchange, double exchange, Zener-RKKY, were suggested to make clear the origin of ferromagnetism, especially in TM doped semiconductors [1, 70-73] including nanowires [74, 75]. Mn-O-Mn favored strongly (relative to Zn-O-Zn) AFM due to superexchange interaction in contrast to distant Mn-Mn pairs which directly interacted through FM. In MnO case, O(p)-Mn(d) hybridization lead pairs to make an FM contribution to the system; herewith, Zn-O-Zn showed weak AFM (Zn-Zn in Table 4). The abovementioned interactions commonly formed the magnetic behavior of the system, FM was preferred; however, several magnetic states exactly existed in the same system.

In the light of obtained magnetic moment (μ_B) and exchange couplings (J) from DFT, magnetic susceptibility (to determine T_c) of nanoparticles which are built on geometry optimized ZnMgMnO supercell, were calculated via Markov Chain Monte Carlo (MCMC) methods based on the Metropolis algorithm detailed in Duru et al. [41]. Thus, transition temperature as a primary parameter for the application of magnetic materials in the device world, namely daily life, was determined by Heisenberg Hamiltonian expressed in equation 2.

$$\mathcal{H} = - \sum J_{ij}(r_{ij}) \mathbf{S}_i \mathbf{S}_j - B \sum S_i^z \quad (2)$$

where S_i and S_j represent the nearest neighboring spins interacting with each other with $J_{ij}(r_{ij})$ exchange energy and B is the applied field. $|S_\alpha|$ was set to 1 and calculated J values (calculated by MFT) were used during the simulation. The thermal equilibrium process took 40% of total MC steps and elapsed time for expectation values was 60% at temperature (T). As shown in Fig. 6, magnetization vs. temperature (M - T) and susceptibility measurements were taken starting from 1K to 800K and the Curie temperature of $Zn_{0.94}Mg_{0.01}Mn_{0.05}O$ was found as 311K, and it is a meaningful value, which is close to room temperature. It is obvious that nanoparticle shows FM behavior directly related to calculated exchange couplings between site atoms below 311K. Note that distant Mn-Mn pairs (>5.8) contributed to FM while AFM behavior started to show up when they come closer. Thus, relatively big nanoparticles would possess FM like behavior in contrast to slightly small ones. Note that, in a previous study, a non-linear intriguing relation between size and magnetic behavior was found [41]. Mg-O pairs contributed to AFM state whereas Mg-Mn pairs interacted FM. This was the reason that why clustered Mg with Mn structure (C1) was preferred to be in FM state.

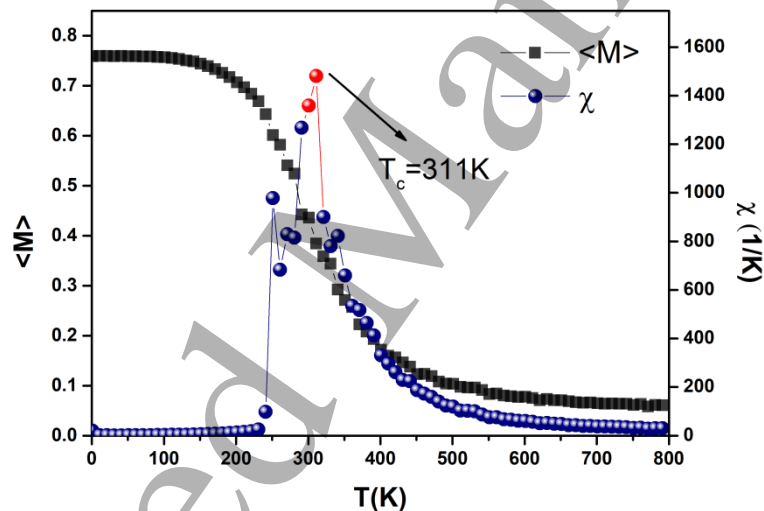


Figure 6. Black squares represent magnetization (M), and blue spheres were used to illustrate magnetic susceptibility (χ) where red spheres point the Curie temperature and the nearest temperature to the Curie temperature (left-sided), respectively, of C1 states of 5% Mn and 1% Mg-doped ZnO.

Conclusion:

The structural and magnetic properties of Mg/Mn-doped ZnO were investigated by the first-principles study and Monte Carlo methods (MCs). Applying magnetic force theorem (MFT) and using Kohn-Sham orbitals in the GGA-PBE scheme, the exchange coupling parameters (J) were calculated to figure out the magnetic interactions between atomic sites

one by one. According to geometry optimization of four different configurations as surface/volume clustered Mn and clustered/non-clustered Mg, Mg-Mn, Mn-Zn, Mn-O, Mg-O, Mg-Zn, Zn-Zn and O-O nearest neighbors came closer except Mn-Mn in Mg clustered structure.

Closest Mn-Mn pair showed strong AFM (bond length $< 3\text{\AA}$) where increasing bond angle and bond length reduced it in contrast to distant Mn ions which were interacted ferromagnetically. Mg-Mn and Mg-Zn pairs not only exhibited FM behavior but also contributed to stabilized ferromagnetism instead of being distant to Mn ions because of the AFM tendency of Mg-O pairs. MnO was strongly ferromagnetic than Mg-Mn. Magnetic behavior of $\text{Zn}_{0.94}\text{Mg}_{0.01}\text{Mn}_{0.05}\text{O}$ was designated by Mn(d)-O(p) hybridization (FM), Mn-O-Mn superexchange (AFM), and Mn-Mn direct exchange (FM) mechanisms. Calculated J values were used to determine T_c of Mg/Mn-doped ZnO nanoparticle via measuring averaged magnetization and magnetic susceptibility. The Curie temperature T_c was found as 311K, which is absolutely above the room temperature.

Acknowledgment

Computing resources used in this work were provided by the National Center for High Performance Computing of Istanbul Technical University, (UHem), Turkey, under grant number 1006342019, the Research Fund of Bahcesehir University (BAU-BAP.2018.02.16), Istanbul, Turkey and the Scientific and Technical Research Council of Turkey (TUBITAK) through the Project No: 115F472.

References

- [1] K. Sato and H. Katayama-Yoshida, Physics, Ab initio Study on the Magnetism in ZnO-, ZnS-, ZnSe- and ZnTe- Based Diluted Magnetic Semiconductors, Phys. Status Solidi B 229 (2002) 673
- [2] Z. L. Wang, Zinc oxide nanostructures: growth, properties, and applications, J. Phys.: Condens. Matter 16 (2004) R829
- [3] S. J. Pearton, D. P. Norton, K. Ip, Y. W. Heo and T. Steiner, Recent progress in processing and properties of ZnO, Prog. Mater. Sci. 50 (2005) 293–340

- 1
2
3
4
5 [4] Ü. Özgür, Y. I. Alivov, C. Liu, A. Teke, M. Reshchikov, S. Doğan, V. Avrutin, S.-J. Cho
6 and H. Morkoc, A comprehensive review of ZnO materials and devices, *J. Appl. Phys.* 98
7 (2005) 11
8
9
10
11 [5] A. Tsukazaki, A. Ohtomo, T. Onuma, M. Ohtani, T. Makino, M. Sumiya, K. Ohtani, S. F.
12 Chichibu, S. Fuke, Y. Segawa, H. Ohno, H. Koinuma and M. Kawasaki, Repeated
13 temperature modulation epitaxy for p-type doping and light-emitting diode based on ZnO,
14 *Nat. Mater.* 4 (2005) 42
15
16
17
18
19 [6] J. Huang, Z. Yin and Q. Zheng, Applications of ZnO in organic and hybrid solar cells,
20 *Energy Environ. Sci.* 4 (2011) 3861–3877
21
22
23
24
25 [7] M. P. Lu, M. Y. Lu and L. J. Chen, p-Type ZnO nanowires: From synthesis to
26 nanoenergy, *Nano Energy* 1 (2012) 247–258
27
28
29
30 [8] H.Y. Guo, Y. Zhao, N. Lu, E. Kan, X.C. Zeng, X.J. Wu, J.L. Yang, Tunable magnetism in
31 a nonmetal-substituted ZnO monolayer: a first-principles study, *J. Phys. Chem. C* 116 (2012)
32 11336
33
34
35
36
37 [9] A. Kołodziejczak-Radzimska, T. Jesionowski, “Zinc Oxide— From Synthesis to
38 Application: A Review”, *Materials MDPI* 7(4) (2014) 2833-2881;
39 <https://doi.org/10.3390/ma7042833>.
40
41
42
43
44 [10] K. P. Shinde, R. C. Pawar, B. B. Sinha, H. S. Kim, S. S. Oh, and K. C. Chung, Study of
45 effect of planetary ball milling on ZnO nanopowder synthesized by co-precipitation, *J. Alloys*
46 *Compd.* 617 (2014) 404–407
47
48
49
50 [11] M Khalid, S Riaz, S Naseem, Tailoring of the Band Gap in Transition Metal-doped ZnO:
51 First Principle Calculations, *Materials Today: Proceedings* 2(10, Part B) (2015) 5246-5250
52
53
54
55 [12] A.S. Fedorov, M.A. Visotin, A.S. Kholobina, A.A. Kuzubov, N.S. Mikhaleva, H.S. Hsu,
56 Investigation of intrinsic defect magnetic properties in wurtzite ZnO materials, *J. Magn.*
57 *Magn. Mater.* 440 (2017) 5-9
58
59
60

- 1
2
3
4
5 [13] J. Kegel, I.M.Povey, M.E.Pemle, Zinc oxide for solar water splitting: A brief review of
6 the material's challenges and associated opportunities, *Nano Energy* 54 (2018) 409-428
7
8
9
10 [14] N. Mamamouni, J.J. Vijaya, A. Benyoussef, A.E. Kenz, M. Bououdina, Electronic
11 structure and magnetic studies of V-doped ZnO: ab initio and experimental investigations,
12 *Bull. Mater. Sci.* 41 (2018) 87
13
14
15
16 [15] Y. Sun, Y. Zong, J. Feng, X. Li, F. Yan, Y. Lan, L. Zhang, Z. Ren and X. Zheng,
17 Oxygen vacancies driven size-dependent room temperature ferromagnetism in well-
18 dispersed dopant-free ZnO nanoparticles and density functional theory calculation, *Journal of*
19 *Alloys and Compounds* 739 (2018) 1080-1088
20
21
22
23
24
25 [16] J. Wu, F. Long, B. Tang, and X. Tang, Electronic structure and ferromagnetic
26 properties of Zn vacancies in ZnO screw dislocations: First-principles calculations, *AIP*
27 *Advances* 8 (2018) 065115
28
29
30
31
32 [17] L. Arda, The effects of Tb doped ZnO nanorod: An EPR study, *J. Mag. Mag. Mater.* 475
33 (2019) 493
34
35
36
37 [18] Y.R. Sui, Y.G. Yue, Y.P. Song, B. Yao, Y. Cao, J.H. Lang, X.Y. Li, J.H. Yang, Cd
38 composition induced effects on structure, optical and electrical properties of sputtered Zn₁₋
39 _xCd_xO films, *Ceram. Int.* 4 (2015) 5414
40
41
42
43
44 [19] D. Akcan, A. Gungor, L. Arda, Structural and optical properties of Na-doped ZnO films,
45 *J. Mol. Struct.* 1161 (2018) 299
46
47
48
49 [20] J. G. Lu, Z. Z. Ye, Y. J. Zeng, L. P. Zhu, L. Wang, J. Yuan, Q. L. Liang, Structural,
50 optical, and electrical properties of (Zn,Al)O films over a wide range of compositions, *J.*
51 *Appl. Phys.* 100 (2006) 073714
52
53
54
55
56 [21] S. A. Wolf, D. Awschalom, R. A. Buhrman, J. M. Daughton, S. V. Molnar, M. L.
57 Roukes, A. Y. Chtchelkanova, D. M. Treger, Spintronics: a spin-based electronics vision for
58 the future, *Science* 294 (2001) 1488
59
60

- 1
2
3
4
5 [22] Y. Ammaih, A. Abderrazak, B. Hartiti, A. Ridah, P. Thevenin, M. Siadat, Structural,
6 optical and electrical properties of ZnO:Al thin films for optoelectronic applications, *Opt.*
7 *Quant. Electron.* 46 (2014) 229 - 234
8
9
10
11 [23] H. Cao, P. Lu, N.Cai, X. Zhang, Z. Yu, T. Gao, S. Wang, First-principles study on
12 electronic and magnetic properties of (Mn, Fe)-codoped ZnO, *J. Mag. Mag. Mater.* 352
13 (2014) 66
14
15
16 [24] I. D.Rezkallah, M.M. Koç, M. Erkovanc, Yu Chumakov d, F. Chemam, Investigation of
17 the electronic and magnetic properties of Mn-doped ZnO using the FP-LAPW method,
18 *Chin. J. Phys.* 55 (2017) 1432-1440
19
20
21 [25] A. El Haimeur, L. El Gana, M. Addou, A. El Kenz, Effect of tuning the structure on the
22 optical and magnetic properties by various transition metal doping in ZnO/TM (TM = Fe,
23 FeCo, Cr, and Mn) thin films, *J. Supercond. Nov. Magn.* 31 (2018) 569-576
24
25
26 [26] S. Xue, F.Zhang, S. Zhang, X. Wang, T. Shao, Electronic and Magnetic Properties of Ni-
27 doped Zinc-Blende ZnO: A First-Principles Study, *Nanomaterials* 8(5) (2018) 281
28
29
30 [27] Z Liu, X Yuan, P Yang, Investigation on electronic and magnetic properties of Co and
31 Mn in ZnO with different doping types, *J. Magn. Magn. Mater.* 461(2018) 1-5
32
33
34 [28] M. V. Gallegos, C. Romina Luna, Miguel A. Peluso, Laura C. Damonte, Jorge E.
35 Sambeth, Paula V. Jasen, Effect of Mn in ZnO using DFT calculations: Magnetic and
36 electronic changes, *Journal of Alloys and Compounds* 795 (2019) 254-260
37
38
39 [29] F. Goumrhar, O. Arybou, E. Salmani, L. Bahmad, H. Ez-Zahraouy, A.
40 Benyoussef, Magnetic Properties of Carbon Co-Doped (Zn,Mn)O Using LDA and LDA-SIC
41 Approximations, *Journal of Superconductivity and Novel Magnetism*, 32 (7) (2019)2275–
42 2281
43
44
45 [30] C. L. Tan, D. Sun, X. H. Tian and Y. W. Huang, Tuning electronic structure and optical
46 properties of ZnO monolayer by Cd doping, *Ceram. Int.* 42 (2016) 10997–11002
47
48
49
50
51
52
53
54
55
56
57
58
59
60

- 1
2
3
4
5 [31] A. Ohtomo, M. Kawasaki, T. Koida, K. Masubuchi, H. Koinuma, Y. Sakurai, Y. Yoshida,
6 T. Yasuda, Y. Segawa, $Mg_xZn_{1-x}O$ as a II–VI widegap semiconductor alloy, *Appl. Phys. Lett.*,
7 72 (1998) 2466
8
9
10 [32] N.B. Chen, H.Z. Wu, D.J. Qiu, T.N. Xu, J. Chen, W.Z. Shen, Temperature-dependent
11 optical properties of hexagonal and cubic $Mg_xZn_{1-x}O$ thin-film alloys, *J. Phys. Condens.*
12 *Matter*, 16 (2004) 2973
13
14
15
16
17 [33] Singh, J. P. and K. H. Chae, Local Electronic Structure Perspectives of Nanoparticle
18 Growth: The Case of MgO, *ACS Omega* 4(4) (2019) 7140-7150
19
20
21
22 [34] H. Chen, C. Tan, D. Sun, W. Zhao, X. Tian and Y. Huang, Ultrawide range tuning of
23 direct band gap in MgZnO monolayer via electric field effect, *RSC Adv.* 8 (2018) 1392-1397
24
25
26
27 [35] OpenMx Ver. 3.8, <http://www.openmx-square.org>
28
29
30
31 [36] Y. Öner, B. Aktaş, “Magnetization measurements and computer simulations for the
32 magnetic hysteresis losses of reentrant $Ni_{100-x}Mn_xPt$ and Ni-Mn alloys”, *Physical Review B*
33 1990, 42 (4), 2425; <https://doi.org/10.1103/PhysRevB.42.2425>
34
35
36
37 [37] S.-R. Liu, H.-J. Zhai, and L.-S. Wang, “s-d hybridization and evolution of the electronic
38 and magnetic properties in small Co and Ni clusters”, *Phys. Rev. B* 65 (2002) 113401;
39 <https://doi.org/10.1103/PhysRevB.65.113401>
40
41
42
43
44 [38] M. El-Hilo, A.A. Dakhel, A.Y. Ali-Mohamed, Room temperature ferromagnetism in
45 nanocrystalline Ni-doped ZnO synthesized by co-precipitation, *J. Magn. Magn. Mater.*, 321
46 (2009) 2279-2283
47
48
49
50
51 [39] L. Arda, M. Açıkgöz, A. Güngör, Magnetic and microstructure properties of ni-doped
52 ZnO films and powder by sol-gel process, *Journal of Superconductivity and Novel Magnetism*
53 25(8), (2012) 2701-2705.
54
55
56
57
58
59
60

- 1
2
3 [40] C. Boyraz, N. Doğan, L. Arda, “Microstructure and magnetic behavior of (Mg/Ni) co-
4 doped ZnO nanoparticles”, *Ceramics International* 43(17) (2017) 15986-15991;
5 <https://doi.org/10.1016/j.ceramint.2017.08.184>
6
7
8
9
10 [41] I.P. Duru, E. Ozugurlu, L. Arda, Size effect on magnetic properties of $Zn_{0.95-x}Mg_xNi_{0.05}O$
11 nanoparticles by Monte Carlo simulation, *Ceram. Int.*45 (2019) 5259-5265
12
13
14
15 [42] A. I. Lichtenstein, M. I. Katsnelson, and V. A. Gubanov, Exchange interactions and spin-
16 wave stiffness in ferromagnetic metals, *J. Phys. F: Met. Phys.* 14 (1984) L125
17
18
19
20 [43] A. I. Lichtenstein, M. I. Katsnelson, V. P. Antropov, and V. A. Gubanov, Local spin
21 density functional approach to the theory of exchange interactions in ferromagnetic metals
22 and alloys, *J. Magn. Magn. Mater.* 67 (1987) 65 - 74
23
24
25
26
27 [44] V. P. Antropov, M. I. Katsnelson, B. N. Harmon, M. vanSchilfgaarde, and D.
28 Kusnezov, Spin dynamics in magnets: Equation of motion and finite temperature effects, *Phys.*
29 *Rev. B* 54 (1996) 1019
30
31
32
33
34 [45] V. P. Antropov, M. I. Katsnelson, and A. I. Lichtenstein, Exchange interactions in
35 magnets, *Physica B* 336 (1997) 237–238
36
37
38
39 [46] B. B. Straumal, A. A. Mazilkin, S. G. Protasova, A. A. Myatiev, P. B. Straumal, G.
40 Schütz, P. A. van Aken, E. Goering, B. Baretzky, Magnetization study of nano grained pure
41 and Mn-doped ZnO films: Formation of a ferromagnetic grain-boundary foam *Phys. Rev. B*
42 79 (2009) 205206
43
44
45
46
47 [47] Stashans, A. and K. Rivera, Electronic and Magnetic Properties of Co- and Mn-codoped
48 ZnO by Density Functional Theory, *Chinese Physics Letters* 33(9) (2016) 097102
49
50
51
52
53 [48] M. F. M. Taib, D. T. Mustafa, N. H. Hussin, M. H. Samat, A. M. M. Ali, O. H. Hassan,
54 M. Z. A. Yahya, First Principles Study on Zn doped MgO using Hubbard U correction,
55 *Materials Research Express* 6 (9) (2019) 2053-1591
56
57
58
59
60

- 1
2
3 [49] I. P. Duru, C. Değer, T. Kalayci, and M. Arucu, “A computational study on magnetic
4 effects of $Zn_{1-x}Cr_xO$ type diluted magnetic semiconductor”, *J. Magn. Magn. Mater.* 396
5 (2015) 268–74; <https://doi.org/10.1016/j.jmmm.2015.08.031>
6
7
8
9
10 [50] K. Lamhal, R. Hayn, A. Boukourt, S. Meskine, L. Abbes and A. Zaoui, Effect of (Co, N)
11 co-doping of p-type ZnO on electronic and magnetic properties by DFT+U studies, *Physica B:*
12 *Condensed Matter* 545 (2018) 491-497
13
14
15
16
17 [51] T. Ozaki, Variationally optimized atomic orbitals for large-scale electronic structures,
18 *Phys. Rev. B.* 67 (2003) 155108
19
20
21
22 [52] T. Ozaki and H. Kino, Numerical atomic basis orbitals from H to Kr, *Phys. Rev. B* 69
23 (2004) 195113
24
25
26
27 [53] T. Ozaki and H. Kino, Efficient projector expansion for the ab initio LCAO method,
28 *Phys. Rev. B* 72 (2005) 045121
29
30
31
32 [54] K. Lejaeghere et al., Reproducibility in density functional theory calculations of solids,
33 *Science* 351 (6280) (2016) aad3000
34
35
36
37 [55] J. P. Perdew, K. Burke, and M. Ernzerhof, Generalized Gradient Approximation Made
38 Simple, *Phys. Rev. Lett.* 77(1996) 3865
39
40
41
42 [56]] H. J. Monkhorst and J. D. Pack, Special points for Brillouin-zone integrations, *Phys.*
43 *Rev. B* 13 (1976) 5188–92.
44
45
46
47 [57] H. Yoon, T. J. Kim, J. H. Sim, S. W. Jang, T. Ozaki, M. J. Han, Reliability and
48 applicability of magnetic-force linear response theory: Numerical parameters, predictability,
49 and orbital resolution, *Physical Review B* 97 (2018) 125132
50
51
52
53
54 [58] Z. Zeng, D. Guenzburger, and D. E. Ellis, Electronic structure, spin couplings, and
55 hyperfine properties of nanoscale molecular magnets, *Phys. Rev. B* 59(1999) 6927
56
57
58
59
60

- 1
2
3 [59] D. W. Boukhvalov, A. I. Lichtenstein, V. V. Dobrovitski, M. I. Katsnelson, B. N.
4 Harmon, V. V. Mazurenko, and V. I. Anisimov, Effect of local Coulomb interactions on the
5 electronic structure and exchange interactions in Mn_{12} magnetic molecules, *Phys. Rev. B*
6 65(2002) 184435
7
8
9
10
11 [60] D. W. Boukhvalov, V. V. Dobrovitski, M. I. Katsnelson, A. I. Lichtenstein, B. N.
12 Harmon, and P. Kögerler, Electronic structure and exchange interactions in V_{15} magnetic
13 molecules: LDA+U results, *J. Appl. Phys.* 93(2003) 7080
14
15
16
17
18 [61] D. W. Boukhvalov et al., Electronic structure of magnetic molecules V_{15} : LSDA+U
19 calculations, x-ray emissions, and photoelectron spectra, *Phys. Rev. B* 67 (2003) 134408
20
21
22
23 [62] V. V. Dobrovitski, H. A. De Raedt, Efficient scheme for numerical simulations of the
24 spin-bath decoherence, *Physical Review E* 67 (2003) 056702
25
26
27
28 [63] M. J. Han, T. Ozaki, J. Yu, Electronic structure, magnetic interactions, and the role of
29 ligands in Mn_n ($n=4, 12$) single-molecule magnets, *Phys. Rev. B* 70 (2004) 184421
30
31
32
33 [64] S. D. Senol, A. Guler, C. Boyraz, L. Arda, Preparation Structure and Magnetic Properties
34 of Mn-Doped ZnO Nanoparticles Prepared by Hydrothermal Method, *Journal of*
35 *Superconductivity and Novel Magnetism*, (2019), *Article In Press*,
36 <https://doi.org/10.1007/s10948-019-5030-7>
37
38
39
40
41
42 [65] Z. K. Heiba and L. Arda, Structural properties of $Zn_{1-x}Mg_xO$ nanomaterials prepared by
43 sol-gel method, *Cryst. Res. Technol.* 44 (2009) 845
44
45
46
47 [66] J. B. Goodenough, An interpretation of the magnetic properties of the perovskite-type
48 mixed crystals $La_{1-x}Sr_xCoO_{3-\lambda}$, *J. Phys. Chem. Solids* 6 (1958) 287–297
49
50
51
52 [67] J. Kanamori, Superexchange interaction and symmetry properties of electron orbitals, *J.*
53 *Phys. Chem. Solids* 10 (1959) 87–98
54
55
56
57 [68] P. W. Anderson, Antiferromagnetism. Theory of superexchange interaction, *Phys. Rev.*
58 79 (1950) 350–356
59
60

1
2
3
4
5 [69] T. Ahmad, S. Khatoon, O. A. Al-Hartomy, Solvothermal synthesis of $Zn_{1-x}Mn_xO$
6 nanoparticles using oxalate precursor route: Optical and magnetic properties, *Arabian Journal*
7 *of Chemistry* 10 (2) (2017) S2138 - S2144
8
9

10
11 [70] H. Akai, Ferromagnetism and its stability in the diluted magnetic semiconductor (In, Mn)
12 As, *Phys. Rev. Lett.* 81 (1998) 3002
13
14

15
16 [71] T. Dietl, H. Ohno, F. Matsukura, J. Cibert, and D. Ferrand, Zener model description of
17 ferromagnetism in zinc-blende magnetic semiconductors, *Science* 287 (2000) 1019
18
19

20
21 [72] A. A. Sasikala Devi and Iman S. Roqan, The origin of room temperature ferromagnetism
22 mediated by Co–VZn complexes in the ZnO grain boundary, *RSC Adv.* 6 (2016) 50818-
23 50824.
24
25
26

27
28 [73] Yufeng Tian et al., Bound magnetic polarons and p-d exchange interaction in
29 ferromagnetic insulating Cu-doped ZnO, *Appl. Phys. Lett.* 98 (2011) 162503.
30
31

32
33 [74] A. A. Sasikala Devi, Udo Schwingenschlögl, Iman S. Roqan, Ferromagnetism in Gd
34 doped ZnO nanowires: A first principles study. *Journal of Applied Physics* 116 (23) (2014)
35 233906.
36
37
38

39
40 [75] A. A. Sasikala Devi and Iman S. Roqan, Defect-impurity complex induced long-range
41 ferromagnetism in GaN nanowires, *Mater. Res. Express*, 2 (2015) 126104.
42
43
44
45
46
47
48
49
50
51
52
53
54
55
56
57
58
59
60